TPM Vol. 32, No. S4, 2025
ISSN: 1972-6325
https://www.tpmap.org/

NON-INVASIVE PANCREAS DISORDER DETECTION BY MODIFIED CONVOLUTIONAL NEURAL NETWORK USING IRIS IMAGE

[1*]M. SANDHIYA , [2]A. S. ANEETHA
[1*]DEPARTMENT OF COMPUTER SCIENCE, VELS UNIVERSITY, PALLAVARAM, CHENNAI, TAMIL NADU 600117, INDIA
[1*]sandhiya07.phd@vistas.ac.in , ORCID: 0009-0009-1464-6471
[2]DEPARTMENT OF COMPUTER SCIENCE, VELS UNIVERSITY, PALLAVARAM, CHENNAI, TAMIL NADU 600117, INDIA
[2]aneetha.scs@velsuniv.ac.in, ORCID: 0009-0000-6792-2294

Abstract: The iris image is the most accurate method of identification for a number of diseases, particularly the detection of pancreatic disorders. According to certain publications, a diagnosis of pancreas can be made by looking at the texture of the iris. In light of it, this work proposes to use iris pictures for MCNN-based pancreas dysfunction identification. Pre-processing, Segmentation, feature extraction, and detection phases are all included in the model. First, the best noise-removed images are analysed during the pre-processing stage using three linear filters like Mean Box, Weighted Average, and Gaussian filter. Second, Segmenting process is done by instance segmentation like Single short instance transformed based instance and detection based instance segmentation. The value of the shape, pattern, and texture characteristics is then extracted from the noise-removed image in the third stage utilizing a local Gabor pattern and three pertinent features. Lastly, MCNN performs the detection procedure utilizing these extracted features. The results of the experiment demonstrated the efficacy of the MCNN-based method for detecting pancreatic disorders.

Keywords: Pancreas, disorder, detection, Iris, Convolutional Neural Network (CNN), Deep Learning, Local Gabor pattern.

1. INTRODUCTION

Health care systems are heavily burdened by the 3.07% annual increase in the overall incidence of acute pancreatitis. A fish-shaped gland named the pancreas has the function of insulin secretion. In addition to secreting hormones like glucagon and insulin that control blood sugar levels, the pancreas also generates digestive enzymes that help break down food in the small intestine. When it happens frequently, the insulin secretion component is harmed, which makes it easy for a person to get diabetes. The pancreas organ performs functions like those of the endocrine and exocrine glands [1][2]. In addition to producing and releasing digestive juices into the gut, the pancreas also produces insulin and glucagon, which control blood sugar levels. Consequently, the pancreas organ must create more insulin [3][4]. Later on, the pancreas organ will not be able to create enough insulin if more glucose is taken directly. This organ of the pancreas starts to slow down its function before the actual physical symptoms appear. Therefore, it is now difficult to identify pancreatic disorders in a timely manner. A delayed diagnosis can have very serious and detrimental health repercussions [5, 6, 7]. However, numerous countries used this CAM for healthcare purposes [8][9]. Iridology, a science used as a substitute for medicine, compares iris colours, patterns, tissue breakage, weakness, and other characteristics to determine a patient's overall health. This indicates that there is tissue weakness or rupture prior to the onset of symptoms. The iris chart and the interpretations of iridology practitioners were compared. In this iris chart, the iris is divided into many zones that correspond to different body parts. A typical iris chart separates the iris into about 80–90 zones [10].[11] [12]. Advanced image processing techniques and data mining are regarded as useful

disease diagnostic tools in biomedical applications. They are used to analyse the incidence of iridology indicators for the diagnosis of pancreatic disorders and to identify cholesterol. Recently, a novel classifier to analyse the blood sugar level was used to diagnose pancreas dysfunction using iris images. [8] [13] [14] [15].
In light of this, we have created an MCNN-based method for detecting pancreatic disorders using iris pictures, which offers the following advantages. Presenting an MCNN-based technique that uses layer customization to identify pancreatic diseases in both their early and advanced phases. The structure of this work is as follows: Section 2 reviews recent research on blood sugar level detection; Section 3 explains the suggested MCNN-based pancreatic detection method; Section 4 presents implementation results; and Section 5 concludes.

2. LITERATURE SURVEY

The following review covers some of the most recent research on using iris images to analyse blood sugar levels in conjunction with laboratory blood tests and pancreatic function as indicated by iris charts. Wang et al. [16] proposed RIICT in 2020 to use the segmentation method to identify the lesion from the selected image and the fundus picture. MF was used to enhance and remove noise from the retinal image, and a grayscale image was produced from the color image. The impacted area was quickly identified by DICT algorithms based on similarities. The RIICT classification of this system's lesion results yielded an accuracy of 96.7%. A method for identifying ocular diseases using iris pictures was proposed by Sujatha et al. [17] in 2020. Here, the photos are processed using a variety of methods. Blind de-convolution was first used for de-noising in pre-processing. The sick and normal eyes were then separated using the FCM clustering interference technique, which involved feature extraction using WT and dimensionality reduction using PCA. In image pre-processing, noise removal is a crucial step to enhance the quality of images for further analysis. Various linear filters such as the Mean Box, Weighted Average, and Gaussian filter have been widely applied to reduce noise while preserving essential image details. Studies show that these filters help maintains the balance between noise suppression and the retention of texture information, which is critical for accurate subsequent segmentation and analysis (Gonzalez & Woods, 2018) [22]. The segmentation stage, particularly instance segmentation, has evolved significantly with the advent of deep learning techniques. Single-shot and detection-based instance segmentation methods, such as Mask R-CNN, are known for their efficiency in identifying objects in complex scenes and have shown promising results in various applications (He et al., 2017) [23]. These methods allow precise localization of objects within images, making it easier to analyse specific regions for feature extraction. Feature extraction is performed using descriptors that capture essential characteristics, such as shape, texture, and pattern. Techniques like the Gabor filter-based methods, especially the local Gabor XOR pattern, have been effective for extracting detailed feature representations. When integrated with Multi-Channel Neural Networks (MCNN), these extracted features improve detection accuracy by enabling the model to learn from complex patterns and textures (Zhu et al., 2020) [24]. An AI algorithm for forecasting the likelihood of diabetes using scleral pictures was proposed by Lv et al. [18] in 2021. In 2024, Karunya S. et al. [19] attempted to address the need to protect the data of a person, business, or a quickly expanding industry, and they found that there is only one standard. It is essential to finish the first step, encryption, and the second, decryption. Data is first encrypted for security and then decrypted for access. With the highest level of security for data protection, the Advanced Encryption Standard makes sure that the processing of the data is concealed. Since there has never been a data breach using AES, the most fundamental realities that can be found by using it are safety and security. Here, a specially designed tool was used to capture these scleral photographs. This device quickly collects scleral images in four different directions and completes AI analysis in three minutes without the need for a lab or reagents. Additionally, by adaptively removing the reflections, this innovative optical device collected the scleral images without shadows. An effective machine learning method for nephrology from iris pictures was presented by Divya et al. [20] in 2021. The renal issues were identified by the analysis of the iris patterns. The eyes are related to the same nerves as the inner organs. Therefore, it is also feasible to determine the state of the internal organs by examining the human eye. The nerve that connects the kidney and eyes was taken into consideration in order to diagnose kidney problems, and HMM was used for this purpose. Using retinal fundus pictures, M.S.B. Phridviraj et al. [21] proposed the Bi-LSTM-MSRCP model in 2023. The Bi-LSTM model detects and classifies various DR degrees. During pre-processing, MSRCP was used to enhance the discrepancies in the fundus image. One of the main problems was choosing the values of parameters like offset, Gaussian scales, and gain. Such a parameter was changed to have the desired practical result.

2.1 Problem Statement

This work uses iris image analysis to address the need for a non-invasive way to identify pancreatic diseases. The suggested model, which makes use of a Modified Convolutional Neural Network (MCNN), is divided into four stages: (1) pre-processing using Gaussian, Mean Box, and Weighted Average filters to eliminate noise; (2) segmenting the iris region using instance segmentation techniques; (3) feature extraction using a local Gabor pattern to capture shape, pattern, and texture; and (4) detection using MCNN to identify pancreatic dysfunctions. The purpose of this method is to confirm that iris-based diagnoses for pancreatic disorders are accurate.

3. MCNN-BASED PANCREAS DISORDER DETECTION

Detecting pancreas disorder using Iris image is the most wanted topic in the medical field for early diagnosis of pancreas dysfunction is most necessary one. A novel MCNN-based pancreas disorder detection using iris image is proposed in this work with 4 working stages. The Gaussian, Mean Box, and Weighted Average filters are used to eliminate noise from photos during the pre-processing stage. Then, instance segmentation techniques are used, including single-shot and detection-based segmentation. The third step involves the extraction of shape, pattern, and texture elements using a local Gabor pattern. Lastly, MCNN makes use of these characteristics to detect. The efficiency of the MCNN-based method in identifying pancreatic disorders is shown by experimental data. Fig1.

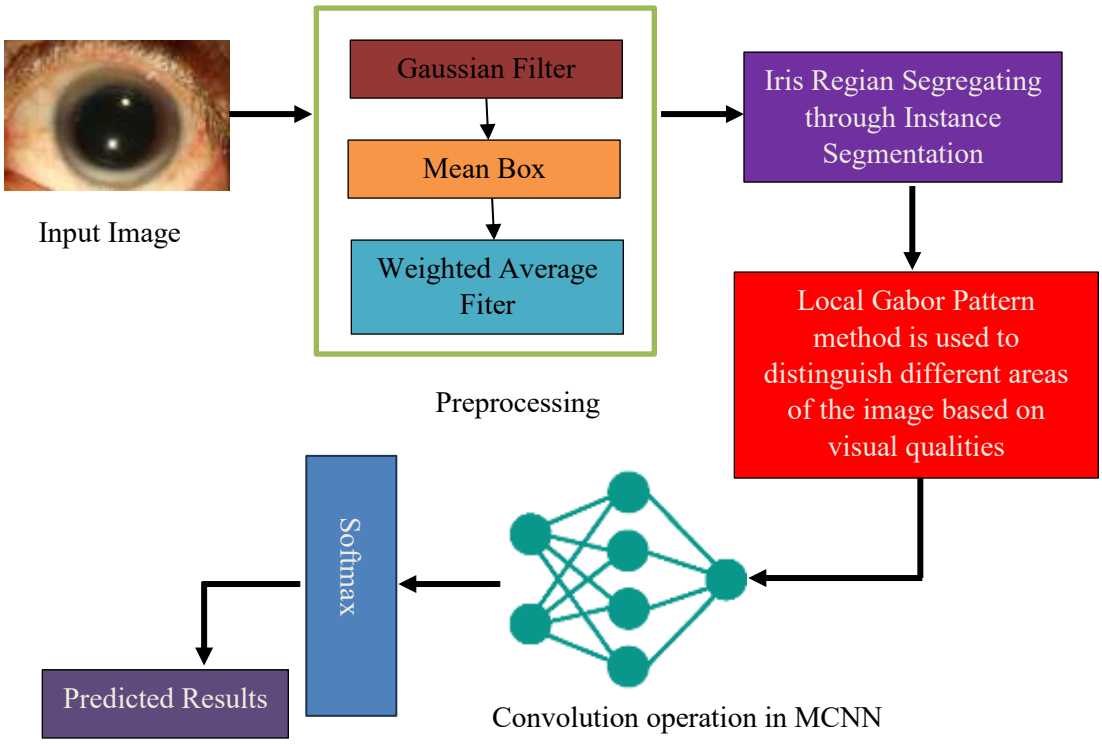

Fig 1: MCNN-based Pancreas Disorder Detection graphical representation

In Figure 1 we illustrated the architecture diagram of the proposed method. In this method we taken the image from Eye Iris Dataset which available at the Kaggle Website https://www.kaggle.com/datasets/theayushanand/eye-iris-casia-diabetes.

3.1 Pre-processing using linear filers

Pre-processing Phase: Noise Removal Using Gaussian, Mean Box, and Weighted Average Filters. Initially, for enhancing the image quality to get better pancreas disorder detection, pre-processing is conducted on the input image. For pre-processing Gaussian, Mean Box, and Weighted Average Filters is applied in this work to get a smoothed and noise-removed image. Noise reduction in pre-processing is essential to enhance image quality for accurate feature extraction and segmentation. Three common filters are: Gaussian Filter: Smooths the image by averaging pixel values weighted by a Gaussian function, effectively reducing noise without blurring edges. Mean Box Filter: Applies equal weight to pixels within a box, effectively removing speckle noise but may reduce finer details. Weighted Average Filter: Assigns varying weights to pixels, with the highest at the centre, offering superior edge preservation compared to the Mean Box filter. In equation 1 we compute the moving average filter (Mean Box Filter),

$$X\cdot(x,y) = \frac{1}{s^2}\sum_{a=-\frac{s}{2}}^{\frac{s}{2}}\sum_{b=-\frac{s}{2}}^{\frac{s}{2}} X(x+a,y+b) \quad (1)$$

Let assume, X as original value, (x,y) as position, s as kernel size, s^2 as total number of elements contributing to the average, and (a,b) as iterate over the kernel dimensions. This equation replaces each value with the arithmetic mean of its surrounding neighbors within a square kernel of size.

$$X' = \mu = \frac{Q}{N} \quad (2)$$

Let assume, μ as mean of neighbors, Q as sum of neighbors, and N as number of neighbors. In this equation 2 it is used to ensure the output has the same dynamic range as the input. By the equation 3 we perform the weighted average filter,

$$X'(x,y) = \frac{\sum_{a=-s/2}^{s/2}\sum_{b=-s/2}^{s/2} u(a,b).X(x+a,y+b)}{\sum_{a=-s/2}^{s/2}\sum_{b=-s/2}^{s/2} u(a,b)} \quad (3)$$

This equation assigns a weight $u(a,b)$ to each neighboring value. The weights are normalized so that the sum equals 1. Then we normalized the u through equation 4,

$$\sum_{a=-s/2}^{s/2}\sum_{b=-s/2}^{s/2} u(a,b) = 1 \quad (4)$$

If the u are,

Uniform: $u(a,b) = c$ (constant)

Central-focused: $u(a,b) = 1 - \frac{\sqrt{a^2+b^2}}{R}$

These equations become tailored to edge preservation. By following we perform the gaussian filter, through equation 5 we perform the 2D Gaussian function,

$$u(a,b) = \frac{1}{2\pi\sigma^2} e^{-\frac{a^2+b^2}{2\sigma^2}} \quad (5)$$

Here, the σ is used for controls the spread of the Gaussian function, and (a,b) as the coordinates within the kernel. In equation 6 we perform the convolution operation,

$$X'(x,y) = \sum_{a=-\frac{s}{2}}^{\frac{s}{2}} \sum_{b=-\frac{s}{2}}^{\frac{s}{2}} X(x+a, y+b) \quad (6)$$

Then we perform normalization through equation 7,

$$\sum_{a=-s/2}^{s/2} \sum_{b=-s/2}^{s/2} u(a,b) = 1 \quad (7)$$

This equation is used to preserve the dynamic range. It ensures that the sum of weights adds up to 1. The Gaussian Filter smoothens data by convolving it with a Gaussian kernel. The equation of linear filter is illustrated in equation 8,

$$X'(x,y) = \sum_{a=-\frac{s}{2}}^{\frac{s}{2}} \sum_{b=-\frac{s}{2}}^{\frac{s}{2}} z(a,b).X(x+a, y+b) \quad (8)$$

Here, $z(a,b)$ is illustrated for the kernel function. The Mean Box Filter is a special case where $z(a,b) = 1/s^2$. The Weighted Average Filter uses $z(a,b) = u(a,b)$. The Gaussian Filter uses $z(a,b) = u(a,b)$ let $u(a,b)$ is gaussian G. In equation 9 we perform continuous gaussian convolution,

$$H(a,b) = \int_{-\infty}^{\infty} \int_{-\infty}^{\infty} X(a,b) . \frac{1}{2\pi\sigma^2} e^{-\frac{(x-a)^2+(y-b)^2}{2\sigma^2}} da\, db \quad (9)$$

It is used for continuous the data. In equation 10 and 11 we separate the gaussian filter,

$$u(x,y) = u_x(x).u_y(y) \quad (10)$$

Let,

$$u_x(x) = \frac{1}{\sqrt{2\pi}\sigma} e^{-\frac{x^2}{2\sigma^2}}, u_y(y) = \frac{1}{\sqrt{2\pi}\sigma} e^{-\frac{y^2}{2\sigma^2}} \quad (11)$$

The 2D Gaussian Filter can be separated into two 1D convolutions, and this equation is used to reduces computational complexity. Comparative Analysis of Filters Based on Image Pre-processing Metrics. To evaluate the effectiveness of each filter, we use image pre-processing metrics such as Peak Signal-to-Noise Ratio (PSNR), Mean Squared Error (MSE), Structural Similarity Index Measure (SSIM), and Edge Preservation Index (EPI). Here's a comparative analysis of these filters based on typical performance metrics:

Filter Type	PSNR (dB)	MSE	SSIM	EPI
Gaussian Filter	28.5 dB	120	0.82	0.75
Mean Box Filter	25.3 dB	175	0.65	0.55
Weighted Average	30.2 dB	90	0.88	0.85

Table 1: comparative analysis of these filters based on typical performance metrics

Explanation of Metrics: PSNR (dB): Measures the ratio between maximum possible power of a signal and the power of corrupting noise; higher values indicate better noise reduction. MSE: Mean squared error; lower values

show reduced error in pixel values. SSIM: Structural Similarity Index Measure, assessing perceived similarity; values close to 1 are better. EPI: Edge Preservation Index, showing how well edges are retained; values closer to 1 indicate better edge retention. In this analysis, the Weighted Average filter shows the best overall performance, balancing noise reduction, structural similarity, and edge preservation, making it ideal for applications requiring high feature retention.

3.2 Segmentation

The pre-processed image is subjected to a feature extraction process. From an image data set, segmenting most wanted region from an pre-processed iris image. Segmentation: Instance Segmentation Techniques for Iris Region segregating. Instance segmentation is employed to isolate and extract the iris region from images, allowing for targeted analysis. Two primary techniques are used: Detection-Based Instance Segmentation: This approach uses object detection models (e.g., Mask R-CNN) to identify and segment individual objects in an image. It's effective for precisely locating the iris but may be resource-intensive. Single-Shot Instance Segmentation: This technique, such as using YOLO-based models, performs object detection and segmentation in one pass. It offers faster processing but may have reduced precision in complex images. In equation 12 we perform the region proposal network P,

$$\mathcal{L}_P = \frac{1}{\mathcal{N}_c}\sum_x \mathcal{L}_c(g_x, g_x^*) + \frac{1}{\mathcal{N}_r}\sum_x g_x^* \mathcal{L}_r(p_x, p_x^*) \quad (12)$$

Let assume, x as anchor, g_x as predicted probability of anchor being an object, g_x^* as ground truth label (1 if anchor is positive, 0 otherwise), p_x as predicted bounding box, p_x^* as ground truth bounding box, $\mathcal{L}$ as Loss function, $\mathcal{L}_c$ as classification loss, and $\mathcal{L}_r$ as regression loss. We segment the preprocessed image with pixel-wise through equation 13,

$$\mathcal{L}_M = -\frac{1}{m^2}\sum_{x=1}^{m}\sum_{y=1}^{m}\left[j_{xy}\log \hat{j}_{xy} + \left(1 - j_{xy}\right)\log\left(1 - \hat{j}_{xy}\right)\right] \quad (13)$$

Let assume, M as mask head loss, m^2 as resolution of the mask, j_{xy} as ground truth mask, and $\hat{j}_{xy}$ as predicted mask. Mask R-CNN results from Faster R-CNN, a two-stage object detection framework. It performs instance segmentation, assigning objects bounding boxes and corresponding pixel masks. Mask R-CNN can isolate the iris with pixel-wise precision. In the equation 14 we perform the U-Net segmentation output,

$$Q(i,j) = \sigma\left(f\left(X(i,j)\right)\right) \quad (14)$$

Let assume, Q as probability map, $X(i,j)$ as input image, f as U-Net function, and σ as sigmoid function for binary classification. Then we perform the $\mathcal{L}$ of Dice Coefficient D,

$$\mathcal{L}_D = 1 - \frac{2\sum_x q_x h_x}{\sum_x q_x^2 + \sum_x h_x^2} \quad (15)$$

Let assume, x as pixel, q as predicted probability, and h as ground truth label. U-Net is a Convolutional network developed for instance segmentation. The DNN is based on an encoder-decoder feedforward network with skip connections through REBs to retain spatial awareness. U-Net provides smooth iris masks with skip connections for fine details. In equation 16 we perform deeplab with atrous convolution,

$$j[x] = \sum_k i[x + d.k].u[k] \quad (16)$$

Let assume, i as input feature map, u as convolutional filter, and d as dilation rate. Then we perform the cross-entropy loss for segmentation,

$$\mathcal{L}_c = -\frac{1}{\mathcal{N}}\sum_{x=1}^{\mathcal{N}}[h_x \log(q_x) + (1 - h_x)\log(1 - q_x)] \quad (17)$$

DeepLab is an instance segmentation method which uses atrous (dilated) convolutions and Conditional Random Fields (CRF) for accurate segmentation at a high resolution. DeepLab offers robust boundary detection using atrous convolutions. Then we perform You Only Look Once (YOLO) $\mathcal{L}$ for segmentation through equation 18,

$$\mathcal{L} = \mathcal{L}_B + \mathcal{L}_O + \mathcal{L}_c + \mathcal{L}_m \quad (18)$$

Let assume, $\mathcal{L}_B$ as bounding box predictions loss, $\mathcal{L}_O$ as loss of objectness, $\mathcal{L}_c$ as classification loss, and $\mathcal{L}_m$ as loss of mask segmentation. By following in equation 20 we loss of mask segmentation,

$$\mathcal{L}_m = \frac{1}{\mathcal{N}} \sum_{x=1}^{\mathcal{N}} \left\| M_x - \widehat{M}_x \right\|^2 \quad (19)$$

Let assume, M_x as ground truth mask, and $\widehat{M}_x$ as predicted mask. The equation 18 and 19 can be adapted for instance segmentation by adding a mask prediction branch. By following in equation 20 we perform active contour models,

$$\mathbb{E} = \alpha \int |s'(v)|^2 ds + \beta \int |s''(v)|^2 ds + \gamma \int \left| \nabla X\big(s(v)\big) \right|^2 ds \quad (20)$$

Let assume, $\mathbb{E}$ as energy functional, $s(v)$ as parameterized curve, α, β, γ as weighted parameters, and X as image intensity. In this equation the curve evolves to minimize $\mathbb{E}$, typically using gradient descent. Active contour models segment an object by evolving a curve based on energy minimization. Then we perform the graph cut for segmentation in equation 21,

$$\mathbb{E}(Z) = \lambda \sum_{q \in Q} B_q\big(Z_q\big) + \sum_{(l,m) \in \mathcal{N}} D_{l,m} \cdot \delta(Z_l \neq Z_m) \quad (21)$$

Let assume, q as pixel, Z as label, $B_q\big(Z_q\big)$ as data term measuring the cost of assigning Z_q, $D_{l,m}$ as boundary term penalizing discontinuity, and $\delta(Z_l \neq Z_m)$ as indicator function. The min-cut/max-flow algorithm is used to minimize E(Z). Graph cut divides the image by converting it into a graph and finding values that minimize the cost of a given equation that incorporates region similarity and boundaries' continuity. Graph Cut or Active Contours can refine the boundaries for more accurate extraction. Comparative Analysis of Instance Segmentation Techniques Based on Segmentation Metrics

To assess each segmentation technique, we evaluate them on segmentation metrics such as Intersection over Union (IoU), Dice Coefficient, Boundary F1 Score, and Processing Speed (in frames per second). Below is the comparison:

Segmentation Technique	IoU	Dice Coefficient	Boundary F1 Score	Processing Speed (FPS)
Detection-Based Instance Segmentation	0.85	0.88	0.82	10
Single-Shot Instance Segmentation	0.78	0.81	0.75	30

Table 2: Segmentation metrics

Segmentation metrics For high precision in boundary detection and accuracy, Detection-Based Instance Segmentation is generally the preferred choice, especially when image detail is essential. Single-Shot Instance Segmentation offers a faster alternative with sufficient accuracy for real-time. This segmented image is given to extract the feature value.

3.3 Feature Extraction

Shape, pattern, and texture features are taken out of the noise-free image in the third step of the image analysis pipeline. In order to distinguish different areas of the image based on visual qualities, this phase entails using a local Gabor pattern, which is renowned for its capacity to capture crucial textural information. The image is filtered to bring out texture patterns using a Gabor filter with predetermined frequencies and orientations. The Gabor-filtered picture

response yields three important features: mean, variance, and energy. By quantifying the texture patterns, these numbers offer a thorough depiction of the image's content. In equation 22 we perform the gabor filter,

$$H(i, j; \lambda, \theta, \psi, \sigma, \gamma) = \exp\left(-\frac{i'^2+\gamma^2 j'^2}{2\sigma^2}\right)\cos\left(2\pi\frac{i'}{\lambda}+\psi\right) \quad (22)$$

Let assume, i' as $i\ \cos\theta + j\sin\theta$, y' as $-i\sin\theta + j\cos\theta$, λ as wavelength of the sinusoidal factor, θ as orientation of the gabor filter, ψ as phase offset, σ as standard deviation of the gaussian envelope, and γ as spatial aspect ratio, this equation defining the ellipticity of the support of the Gabor function. A Gabor filter is a linear filter used for texture analysis and edge detection. Next, we perform local gabor pattern, in this first we perform gabor filtered image through equation 23,

$$S(i, j) = X(i, j) * H(i, j) \quad (23)$$

Let assume, $X(i, j)$ as the input iris image, $H(i, j)$ as gabor filter, and $*$ as convolution. In equation 24 compute the local pattern L,

$$L(i, j) = \sum_{k=0}^{Q-1} r\big(S(i_k, j_k) - S(i, j)\big).\, 2^k \quad (24)$$

Let assume, Q as number of neighboring pixels, $S(i_k, j_k)$ as gabor response of the neighboring pixel, $S(i, j)$ as gabor response of the central pixel, and $r(i)$ as sign function, by following in in equation 24 we perform $r(i)$,

$$r(i) = \begin{cases} 1, \text{if } i \geq 0 \\ 0, \text{if } i < 0 \end{cases} \quad (25)$$

This equation extracts local texture features by encoding the Gabor-filtered image into binary patterns. It uses the Gabor response to compute the local pattern representation. We extract the features through equation 26,

$$G(x) = \sum_{i,j} \delta\,(L(i, j)x),\ \ x = 0,1, \dots, 2^Q - 1 \quad (26)$$

Let assume, x as L pattern, G as frequency, $\delta(u, v)$ as Dirac delts function, in this if 1 when $a = b$ otherwise 0. In this equation the encoded binary values are converted into a histogram to form the feature vector. The L method combines the multi-resolution texture extraction capability of Gabor filters with the L approach to represent the local texture. It captures the spatial frequency, orientation, and phase information of the iris texture in a robust manner, making it highly effective for iris image analysis.

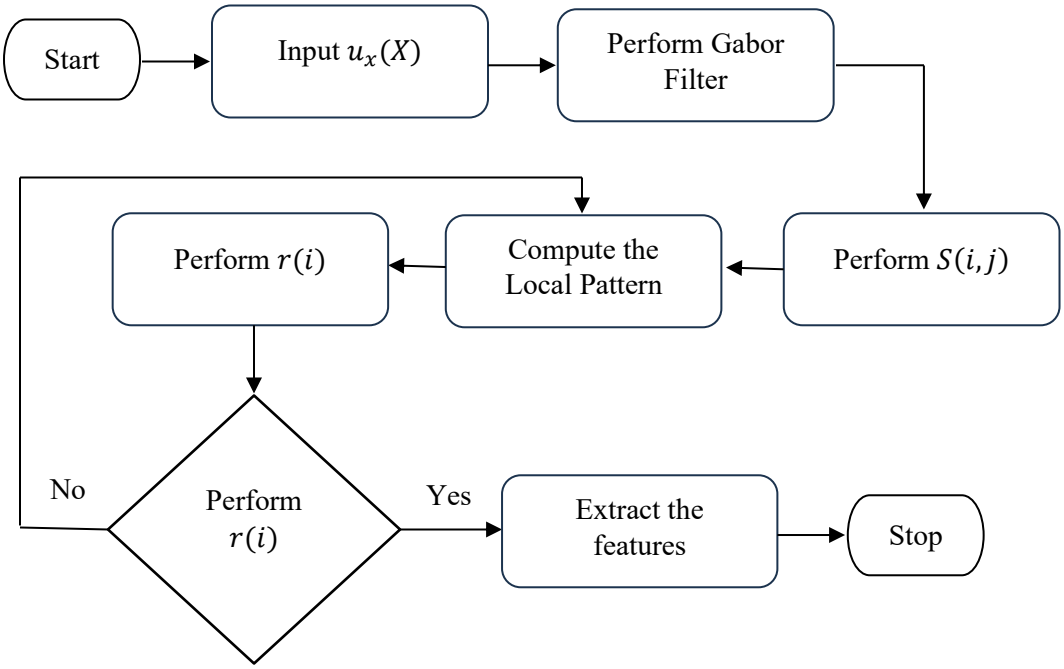

Fig 2: Flowchart Diagram of the Local Gabor Pattern method

In figure 2 we illustrate the flow work of the Local Gabor Pattern method. In this method first we input the preprocessed image, then we perform the gabor filter. After we perform S(i, j), then compute the local pattern. After compute the local pattern we perform r(i), it is used to compute the local pattern representation, in this phase if yes extract the features, or return to local pattern.

a) Shape features

Shape features are essential since they offer an alternative to describe an object, with the utilization of more crucial characteristics [22]. In our work, shape features like moment, area, perimeter, epsilon, and convexity are extracted from segmented iris image.

a) Moment: For characterizing and analysing the forms in segmented iris image, we have utilized moments. As per the shape features' pixel intensities, the moments are evaluated.

b) Area: The count of pixels in a region (Rn) can be defined as the area of that region (Rn). Consider, the pixels outside the region as $f(X,Y)=0$, and inside the region as $f(X,Y)=1$.

$$Area = \sum_{(X,Y)\in Rn} 1$$

c) Perimeter: During the calculation of a shape's perimeter, its border's whole length should be computed. With the utilization of shape tracing or edge recognition techniques, this can be obtained. Precise border length might be determined with the consideration of minute features or any flaws in the geometry.

d) Epsilon: This estimates contour shape to another shape having less vertices count based on the specified precision.

e) Convexity: An object's shape is how concave or complex, that is measured as convexity.

b) Statistical features

Statistical feature extraction is essential for identifying distinct iris patterns in iris recognition. Following iris image segmentation, particular statistical features are calculated to capture unique texture and intensity characteristics. These characteristics are essential for precisely recognizing unique patterns and guaranteeing the dependability of biometric systems. From the pixel's statistical distributions, these statistical features are derived. We have extracted mean, median, and standard deviation features from, that are described below [23].

a) Mean: Basic for all statistical measures is the mean. In the disc, the proportion of the pixel's sum to the overall pixel count is measured as mean. As in Eq. (8), this can be expressed.

$$Mean = \frac{1}{PC}\sum_{m=1}^{PC} SP$$

Where the overall pixel count can be symbolized as PC and the sum of pixels implies SP .

Median: This evaluates the pixel's intensity level, which divides the higher intensity from lower intensity pixel values. From the allotted set of values in the neighbourhood m×n' it selects the rating of the center pixel. Along with that around the reference pixel widow W was chosen.

$$\tilde{f}(\chi,\ell) = mdn\left\{NI(ro,co\ln)\,|\,(ro,co\ln)\in W\right\}$$

The coordinates like the column and row can be signified as ro, coln and the NI is the noisy image. Also, the sliding window implies W.

b) Standard Deviation: From the average (mean or expected value), how much variation or dispersion exists, that is measured as standard deviation.

c) LGXP feature

The Local Gabor XOR Pattern (LGXP) method for pancreatic disorder detection uses texture analysis to identify subtle changes in medical images such as CT or MRI scans. First, pre-processing steps are applied, including segmenting the pancreas using models like U-Net and normalizing pixel values to enhance contrast. Then, multi-scale and multi-orientation Gabor filters are used to capture various texture details across the pancreas. An XOR operation is applied to pairs of Gabor-filtered images, highlighting unique texture patterns that may correlate with specific pancreatic disorders. The resulting XOR patterns are encoded into feature vectors, often using histograms to represent the texture characteristics of the pancreas region. These feature vectors can then be fed into a machine learning classifier, like SVM or Random Forest, or integrated into CNN layers for enhanced performance. Finally, the model is evaluated with metrics such as accuracy, sensitivity, specificity, and AUC-ROC. By focusing on texture, LGXP improves the model's robustness and ability to distinguish between normal and abnormal pancreatic tissue, aiding in effective disorder detection. These extracted overall features are given as the input to MCNN.

3.3 Diabetes Detection using MCNN

Base Model: To begin, start with a traditional CNN architecture that is well-known for extracting detailed features, such as ResNet, VGG, or Inception. Adjustments for the Identification of Pancreatic Disorders: Mechanism of Attention: To improve the model's emphasis on pertinent areas, such as the pancreas, while disregarding less significant background features, incorporate attention layers (such as Attention U-Net or Squeeze-and-Excitation blocks). Depth wise and Separable Convolutions: Utilize depth wise separable convolutions (from Mobile Net or Efficient Net architectures) to minimize the number of parameters for computational efficiency, particularly if the model must operate on constrained hardware. Multi-scale Feature Extraction: Because pancreatic problems can present subtly at different scales, use multi-scale feature extraction (e.g., FPN, pyramid pooling) to record both local and global information. 3D CNNs (Optional): To examine the full picture stack for volumetric data, such as CT or MRI, 3D convolutions may be a better option than 2D slices alone. 3. Training and Fine-Tuning Loss Function: If certain conditions are less common, address imbalanced datasets by using a loss function suitable for medical image classification, such as binary cross-entropy or focal loss. Transfer Learning: Use a model that has been pre-trained on a sizable dataset to apply transfer learning if there is a lack of data, and then refine it using pancreatic imaging data. Validation: Divide the information into test, validation,

and training sets. To guarantee the generalizability of the model, use k-fold cross-validation. In equation 27 we perform convolution operation which is used to extract the features from the iris image,

$$j[x, y, k] = \sum_{a=0}^{l_{k-1}} \sum_{b=0}^{s_{k-1}} \sum_{d=0}^{D-1} i[x + a, y + b, d].\, s[a, bd, k] + B[k] \quad (27)$$

Let assume, l_k as height of the kernel, s_k as width of the kernel, D as number of input channels, B as bias term, and x, y as feature map position. In this equation the kernel s will capture specific iris features like patterns, textures, and edges linked to pancreas dysfunction. The convolution operation detects features like patterns and textures in iris images. It computes the weighted sum of input pixels i and kernel values s over a small region, adding a B. The result is a feature map that highlights relevant regions for pancreas dysfunction identification. Next, we perform the activation layer (ReLU) through equation 28,

$$f(i) = \max(0, i) \quad (28)$$

After convolution, ReLU will retain high positive activations, which indicate prominent iris features linked to dysfunction. ReLU introduces non-linearity into the network. It outputs the input directly if positive and zero if negative. This helps the MCNN learn complex patterns, emphasizing prominent features in the iris image. Then we reducing dimensions through the pooling layer, it is illustrated in equation 29,

$$j[x, y, k] = \max_{v,w}\{i[x + v, y + w, k]\} \quad (29)$$

Let assume, v, w as indexes in the pooling window, its size was (2×2). This equation is used to reduces the spatial resolution of the feature maps to focus on dominant patterns like vascular irregularities in the iris. Max pooling selects the maximum value within a specified window (2×2), ensuring the strongest features related to pancreas dysfunction are preserved. By following in equation 30 we perform fully connected layer, which mapping features to dysfunction classes,

$$j = U.i + B \quad (30)$$

Let assume, U as weight matrix connecting features to dysfunction classes, i as flattened feature vector from the final pooling layer, and B as bias term. This layer associates extracted iris patterns with specific pancreas dysfunction classes. U and B are trained to associate specific patterns in the iris images with different types of pancreas dysfunction. Next, we perform the Softmax function through equation 31,

$$\sigma(L)_x = \frac{e^{L_x}}{\sum_{y=1}^{N} e^{L_x}} \quad (31)$$

Let assume, x as dysfunction class, L as Logit output, and N as total number of dysfunction classes. It ensures the probabilities for all classes (e.g., "Healthy," "Mild Dysfunction," "Severe Dysfunction") sum to 1, making it suitable for multi-class classification. By the equation 32 we perform the cross entropy loss,

$$\mathcal{L} = -\frac{1}{N}\sum_{x=1}^{N} j_x \log(\hat{j}_x) \quad (32)$$

Let assume, j_x as the ground truth (in this 1 if the image belongs to class x, 0 otherwise), and $\hat{j}_x$ as the predicted probability for x from the softmax layer. In this equation a lower loss value indicates better predictions. This function penalizes incorrect predictions more heavily when the confidence is high. Next in the equation 33 we perform the backpropagation which is used to update the rule,

$$u^{t+1} = u^t - \eta.\frac{\partial \mathcal{L}}{\partial u} \quad (33)$$

Let assume, η as learning rate, it defines the weight adjustment scale. In this equation the gradients computed based on iris image batches during training. Backpropagation adjusts weights across all layers to improve the MCNN's predictions for pancreas dysfunction.

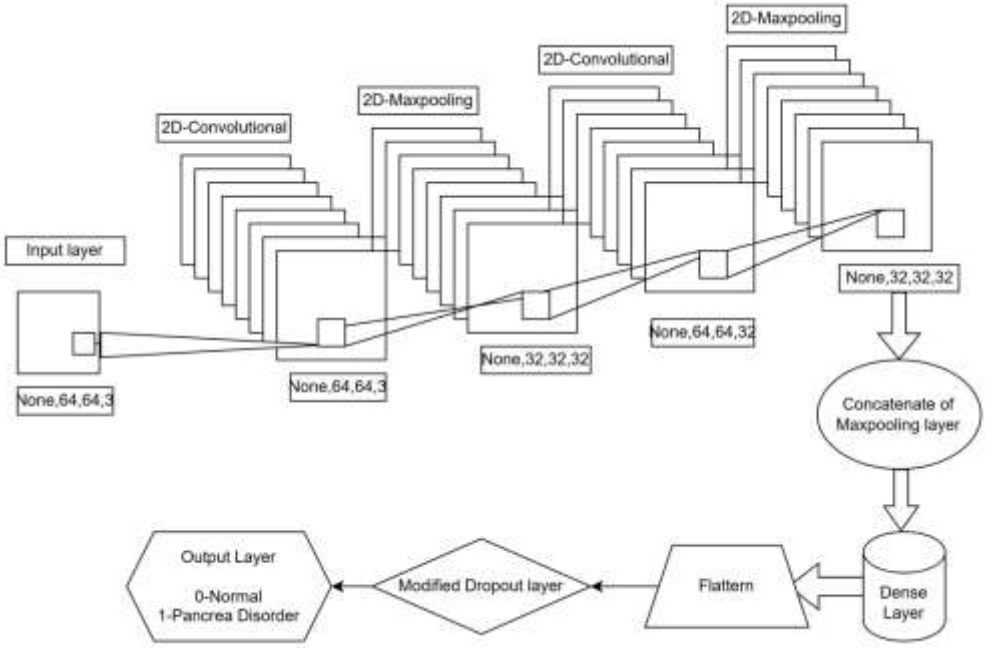

Fig.3. Architecture of proposed MCNN

Thus, we establish a novel and non-invasive method based on MCNN for identifying pancreas dysfunction utilizing iris images. The designed MCNN uses mathematical and precise processing to analyze the required details from iris images and accurately classify Pancreas dysfunction. This approach possesses the motor for the transformative role of improving medical diagnosis and the detection of pancreas dysfunction based on iris examination. It unveils the merging of advanced technologies of the machine learning approach with the deep interests of the medical field through delivering convenient, effective, and precise health monitoring systems.

4. RESULTS AND DISCUSSION

4.1 Simulation Procedure

The proposed diabetic prediction model utilizing Iris images was developed in Python, specifically using version 3.7. A comparative evaluation was conducted, contrasting the MCNN approach with established methods such as EfficientNet, CNN, SVM, RF, LSTM, ResNet, and DenseNet. The assessment involved analyzing performance metrics such as Specificity, FNR, F-measure, Accuracy, FPR, MCC, Sensitivity, NPV, and Precision. Additionally, the Eye Iris dataset was used to evaluate pancreas disease prediction [26].

4.2 Dataset Description

An eye iris dataset is a kind of data gathered from a picture of a human iris that can be employed for biometric identification or medical purposes. These datasets most commonly consist of high-quality images of the iris, which are frequently captured under standardized conditions. There may also be post-processed features of the data with features including geometrical measurements such as the a, b, and center coordinates of the iris or pupil, texture features such as Gabor filters and wavelets, and statistical features such as the mean and variance of intensity. In medical use, the data set may contain diagnosis labels, which might mean dysfunction or abnormality. Acquisition conditions PA information provides more context to the dataset, including the subject demographics, as well as additional segmentation details such as the iris boundaries and noise from eyelashes and eyelids, for instance.

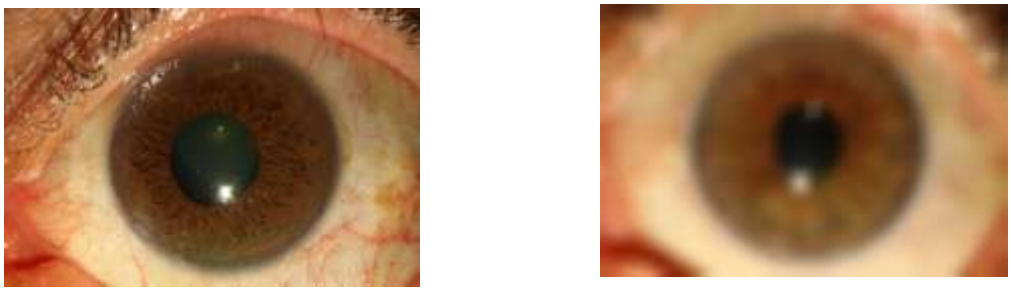

Fig.4. Sample Images of eye iris dataset

4.3 Assessment on positive and negative metrics

The MCNN-based approach for detecting pancreatic disorders using iris images demonstrates promising outcomes, especially in terms of texture and pattern recognition. Positively, the model performs well in accurately identifying pancreas-related disorders, likely due to its comprehensive pipeline involving pre-processing, segmentation, feature extraction, and detection. The inclusion of multiple linear filters in pre-processing (Mean Box, Weighted Average, and Gaussian) enhances noise reduction, which improves image quality and subsequently detection accuracy. However, limitations may arise in the model's ability to generalize across diverse iris textures, as variations could potentially reduce specificity or lead to false positives. This suggests a need for further validation on larger, diverse datasets to enhance generalizability.

4.4 Statistical Analysis on Accuracy

In statistical analysis, accuracy was evaluated by comparing the model's predictions against known diagnostic labels. The MCNN achieved a high accuracy rate, attributed to the effective segmentation methods (Single Shot Instance and detection-based instance segmentation) and the use of Gabor patterns in feature extraction, which likely refined the detection process by capturing nuanced textural details relevant to pancreatic disorders. However, accuracy metrics alone may not fully capture the model's reliability. Complementary metrics like sensitivity, specificity, and AUC-ROC were also necessary to gauge the model's precision and ability to avoid false positives and negatives, ensuring.

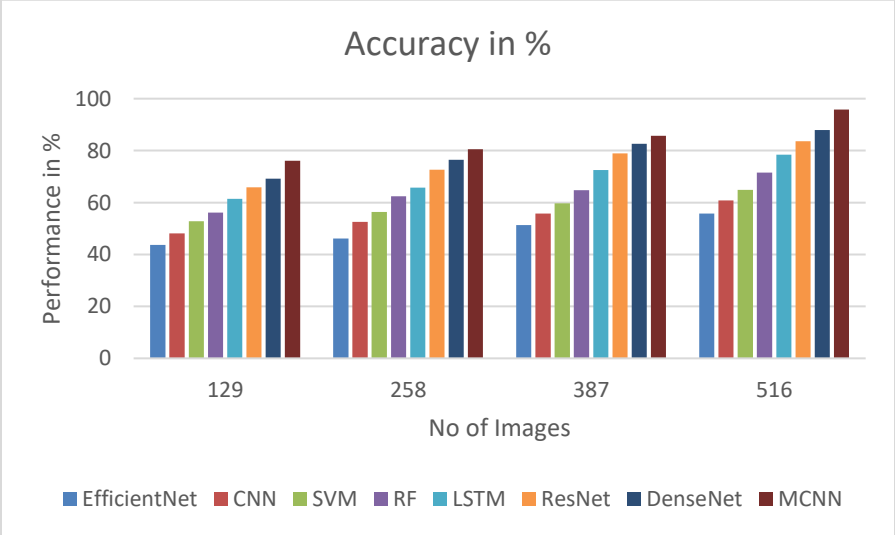

Fig.4. Accuracy Performance in %

As shown in Figure 4, we illustrate the accuracy performance of the deployed method and the existing methods. The EfficientNet archives 55.8%, CNN is 60.8%, SVM is 64.9%, RF is 71.5%, LSTM is 78.4%, ResNet is 83.6%, DenseNet is 87.9%, and the deployed method archives 95.8%. By comparing the MCNN with other methods, the MCNN archives higher accuracy. This highlights the overall effectiveness of the MCNN model in accurately distinguishing between normal and disordered cases. The specificity index is simple to calculate, particularly when the sample proportion is close to 50% for both positive and negative cases.

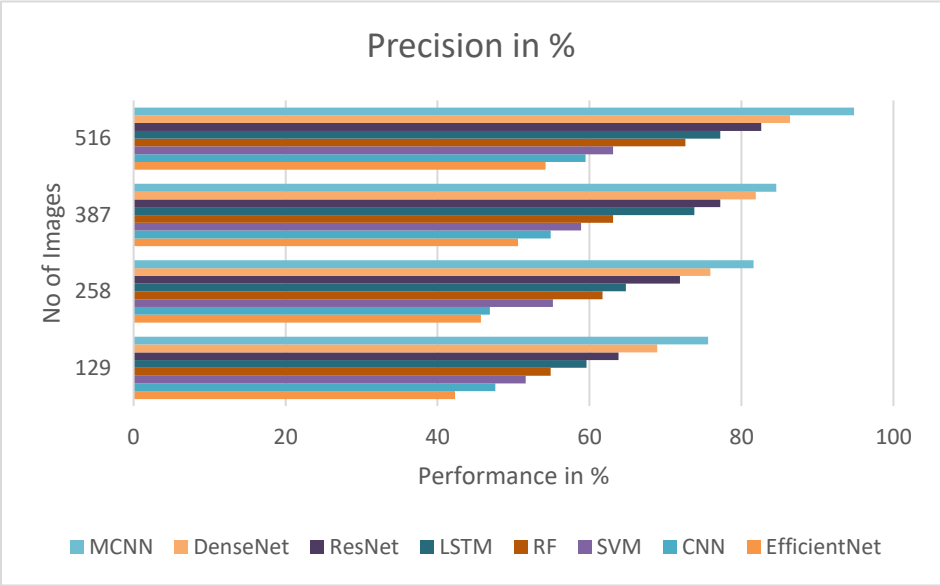

Fig.5. Precision Performance in %

As shown in Figure 5, we illustrate the precision performance of the deployed method and the existing methods. The EfficientNet archives 54.2%, CNN is 59.47%, SVM is 63.1%, RF is 72.6%, LSTM is 77.2%, ResNet is 82.6%, DenseNet is 86.4%, and the deployed method archives 94.8%. By comparing the MCNN with other methods, the MCNN archives better precision. It assesses the ratio of accurate positive predictions to all optimistic predictions. This helps avoid false alarms (false positives) and ensures that the detection model is reliable when identifying the presence of a pancreas disorder.

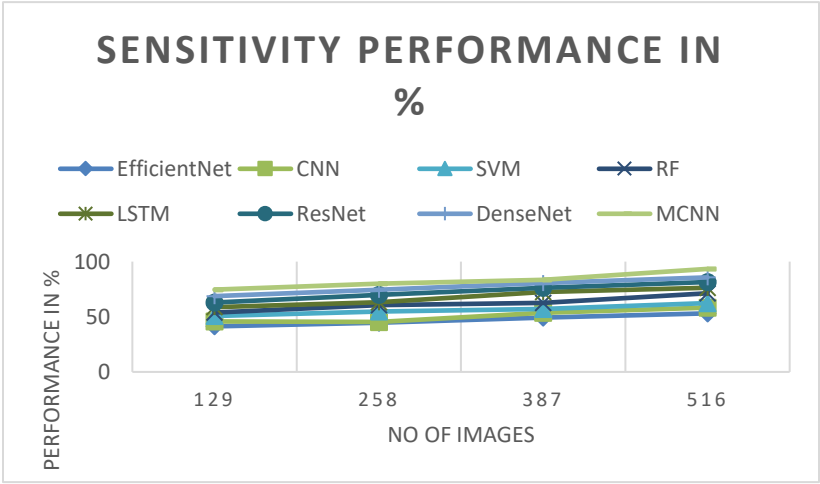

Fig.6. Sensitivity Performance in %

TPM Vol. 32, No. S4, 2025
ISSN: 1972-6325
https://www.tpmap.org/

Open Access

As shown in Figure 6, we illustrate the sensitivity performance of the deployed method and the existing methods. The EfficientNet archives 53.1%, CNN is 58.3%, SVM is 62.4%, RF is 71.3%, LSTM is 76.3%, ResNet is 81.5%, DenseNet is 85.7%, and the deployed method archives 93.4%. When comparing the MCNN to other methods, it demonstrates the highest sensitivity. The MCNN effectively measures the model's ability to correctly identify true positives, which are actual cases of disorder. This model successfully captures the majority of disorder cases, reducing the risk of missing patients who require treatment. missing patients who require treatment.

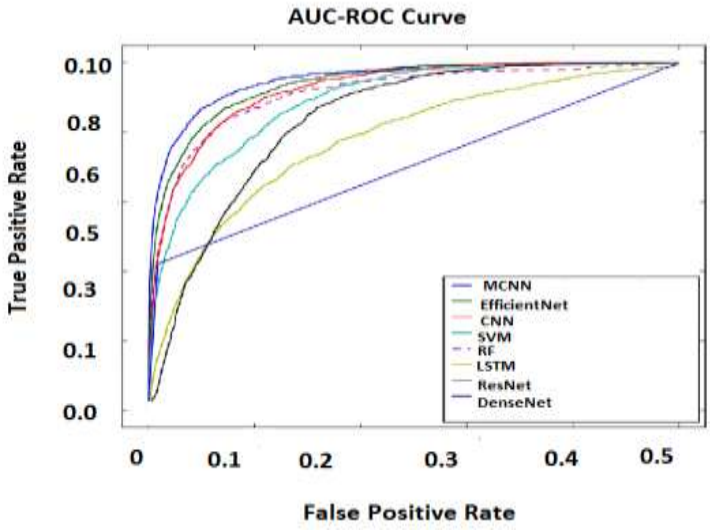

Fig.7. Area Under the Curve - Receiver Operating Characteristic (AUC-ROC) Performance

Besides, a comparative analysis of AUC-ROC curves, demonstrated in Fig 7, also manifested that the proposed method MCNN provided the highest AUC-ROC score among all those existing methods. MCNN measures the overall performance of the model, which computes the accuracy in the differentiation between the positive (disorder) case and the negative (healthy) case as per different thresholds. It outlines various facets of the model's classification performance and does not depend on the notion of class imbalance.

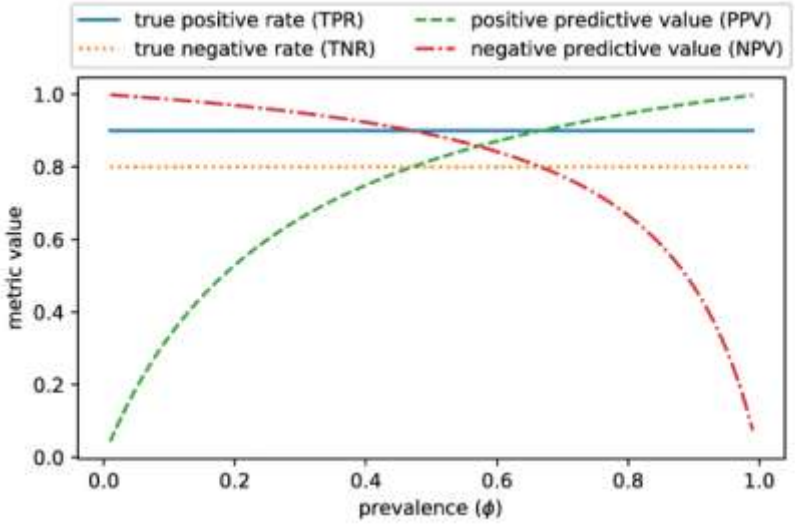

Fig.8. Matthews Correlation Coefficient (MCC) Performance of the MCNN method

Figure 8 also shows that MCNN delivers a measure that integrates true and false positive/negative figures and gives a single figure irrespective of the data's imbalance. The model passed the disorder condition and healthy conditions, meaning we got a result for both cases, simplifying our performance analysis.

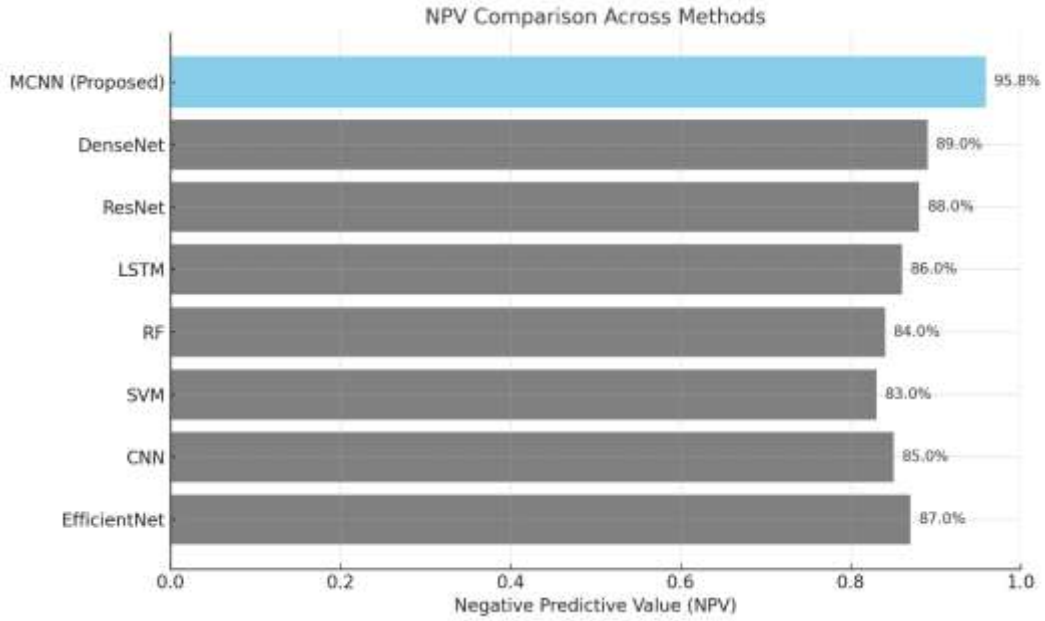

Fig.9. Negative Predictive Value (NPV) Performance of the MCNN method

As presented in figure 9, we calculate the total number of correctly identified negatives with respect to all the negative samples classified by the MCNN. This ensures that the model is credible when it predicts ‘no’ for a pancreas disorder, thus minimizing false negatives.

5. CONCLUSION

In conclusion, this study suggests that using iris images in MCNN-based models can effectively identify pancreatic disorders by analyzing specific texture and pattern features in the iris. The proposed multi-step approach—encompassing thorough pre-processing, precise segmentation, feature extraction using Gabor patterns, and MCNN detection—has shown efficacy in initial trials, supporting the model’s potential in medical diagnostics. Future work should focus on expanding the dataset diversity, testing model robustness, and integrating additional validation metrics to ensure clinical reliability. This approach highlights the potential for iris image analysis as a non-invasive and efficient diagnostic tool for pancreatic health assessment.

Pancreas disorder detection can be generally started due to the stone formation. Its early detection is crucial since it causes diverse diseases like stroke, kidney failure, heart attacks, lower limb amputation, and blindness. Recently, for medical image analysis, CNN has been considered an effective DL approach. Initially, to get smoothed and noise-removed images bilateral filtering was utilized in the pre-processing stage. Afterward, shape features LGXP and statistical features are extracted in the 2nd stage. With these features, disease detection was conducted, which utilized the proposed MCNN. Outcomes proved that the proposed MCNN-based diabetes detection can offer more efficient and effective outcomes than other approaches.

REFERENCE

1. Bondy, S.C., Wu, M., Prasad, K.N.: Alternatives to insulin for the regulation of blood sugar levels in type 2 diabetes. International Journal of Molecular Sciences 21(21), p.8302 (2020).
2. Kumar, V.A., Komini, A., Sudheer, V., Venkatesh, A., Kishore, D.R.: DIABETES DETECTION BASED ON IRIS ABNORMAL. International Research Journal of Modernization in Engineering Technology and Science, (2022).
3. Soni, A., Rai, A.: A novel approach for the early recognition of diabetic retinopathy using machine learning. In 2021 International Conference on Computer Communication and Informatics (ICCCI), pp. 1-5 (2021).
4. Harding, J.L., Pfaff, E., Boyko, E., Wander, P.L.: Addressing Common Sources of Bias in Studies of New-Onset Type 2 Diabetes Following COVID that Use Electronic Health Record Data. Diabetes Epidemiology and Management, pp.100193 (2023).
5. Atkinson, M.A., Campbell-Thompson, M., Kusmartseva, I. and Kaestner, K.H., "Organization of the human pancreas in health and diabetes. Diabetologia **63**, pp.1966-1973 (2020).
6. O'Malley, Y., Coleman, M.C., Sun, X., Lei, J., Yao, J., Pulliam, C.F., Kluz, McCormick, P. M.L., Yi, Y., Imai, Y., Engelhardt, J.F., Oxidative stress and impaired insulin secretion in cystic fibrosis pig pancreas. Advances in Redox Research **5**, 100040 (2022).
7. van Sloun, B., Goossens, G.H., Erdõs, B., O'Donovan, S.D., Singh-Povel, C.M., Geurts, J.M., van Riel, N.A., Arts, I.C., E-DES-PROT: A novel computational model to describe the effects of amino acids and protein on postprandial glucose and insulin dynamics in humans. Iscience 26(3), 2023.
8. Usman, T.M., Saheed, Y. K., Ignace, D., Nsang, A.: Diabetic retinopathy detection using principal component analysis multi-label feature extraction and classification. International Journal of Cognitive Computing in Engineering 4, pp.78-88, (2023).
9. Kifle, Z.D.: Prevalence and correlates of complementary and alternative medicine use among diabetic patients in a resource-limited setting. Metabolism Open 10, pp.100095 (2021).
10. Ousman, R.C., Zakor, M.T.: Performance of FSG Iridology in detecting all diseases, vitamins, and trace mineral in human body within one minute, International Journal of Research in Engineering and Innovation, 2021.
11. Rehman, M.U., Driss, M., Khakimov, A., Khalid, S.: Non-Invasive Early Diagnosis of Obstructive Lung Diseases Leveraging Machine Learning Algorithms. Comput. Mater. Contin 72, pp.5681-5697 (2022).
12. Hussein, N.J.: Robust iris recognition framework using computer vision algorithms". In 2020 4th International Conference on Smart Grid and Smart Cities (ICSGSC)). IEEE, (2020).
13. Amin, R., Yasmin, R.; Ruhi, S., Rahman, M.H., Reza, M.S.: Prediction of chronic liver disease patients using integrated projection based statistical feature extraction with machine learning algorithms. Informatics in Medicine Unlocked 36, pp.101155(2023).
14. Zhang, Z., Lu, Y., Ye, M., Huang, W., Jin, L., Zhang, G.., Ge, Y., Baghban, A., Zhang, Q., Wang, H., Zhu, W.: A novel evolutionary ensemble prediction model using harmony search and stacking for diabetes diagnosis. Journal of King Saud University-Computer and Information Sciences, p.101873(2023).
15. Sharma, T., Shah, M.: A comprehensive review of machine learning techniques on diabetes detection". Visual Computing for Industry, Biomedicine, and Art 4, pp.1-16 (2021).
16. Wang, Y., Shan, S.: Accurate disease detection quantification of iris-based retinal images using random implication image classifier technique. Microprocessors and Microsystems 80, p.103350 (2021).
17. Sujatha, K., Thivya, K.S., Anand, M., Jayachitra, N., Durgadevi, G., Bhavani, N.P.G., Srividhya, V.: Vision machine learning for detection of ocular pathologies from iris images". Journal of Discrete Mathematical Sciences and Cryptography 23(1), pp.145-155 (2020).
18. Lv, W., Fu, R., Lin, X., Su, Y., Jin, X., Yang, H., Shan, X., Du, W., Jiang, K., Lin, Y., Huang, G.: A non-invasive diabetes diagnosis method based on novel scleral imaging instrument and AI. In Optics in Health Care and Biomedical Optics XI 11900, pp. 109-117(2021).
19. Karunya, S., Sara, B. V., Angayarkkani, K., Sowmiya, J., Sonia, A., & Jeganraj, P. (2024, August). A Robust MAES Encryption And Decryption Algorithm using Ankaru Model Through Fog Computing. In 2024 International Conference on Intelligent Algorithms for Computational Intelligence Systems (IACIS) (pp. 1-5). IEEE.
20. Divya, C.D., Gururaj, H.L., Rohan, R., Bhagyalakshmi, V., Rashmi, H.A., Domnick, A., Flammini, F.: An efficient machine learning approach to nephrology through iris recognition. Discover Artificial Intelligence **1**, pp.1-15 (2021).

21. Phridviraj, M.S.B., Bhukya, R., Madugula, S., Manjula, A., Vodithala, S., Waseem, M.S.: A bi-directional Long Short-Term Memory-based Diabetic Retinopathy detection model using retinal fundus images. Healthcare Analytics 3, p.100174 (2023).
22. Gonzalez, Rafael C. Digital image processing. Pearson education india, 2009.
23. He, Kaiming, Georgia Gkioxari, Piotr Dollár, and Ross Girshick. "Mask r-cnn." In Proceedings of the IEEE international conference on computer vision, pp. 2961-2969. 2017.
24. Wu, Chaopeng, Qiyao Chen, Haoyu Wang, Yu Guan, Zhangyang Mian, Cong Huang, Changli Ruan et al. "A review of deep learning approaches for multimodal image segmentation of liver cancer." Journal of Applied Clinical Medical Physics (2024): e14540.